Line-scanning detection instrument for photonic crystal enhanced fluorescence

Vikram Chaudhery,[1] Meng Lu,[1] Cheng-Sheng Huang,[1] James Polans,[1] Ruimin Tan,[2] Richard C. Zangar,[2] and Brian T. Cunningham[1,3,*]

[1]*Department of Electrical and Computer Engineering, University of Illinois at Urbana–Champaign, Urbana, Illinois, USA*

[2]*Pacific Northwest National Laboratory, 902 Battelle Boulevard, Richland, Washington 99354, USA*

[3]*Department of Bioengineering, University of Illinois at Urbana–Champaign, Urbana, Illinois, USA*

**Corresponding author: bcunning@illinois.edu*

Received February 16, 2012; revised May 4, 2012; accepted May 6, 2012;
posted May 7, 2012 (Doc. ID 163203); published June 21, 2012

A laser line-scanning instrument was developed to optimize the near-field enhancement capability of a one-dimensional photonic crystal (PC) for excitation of surface-bound fluorophores. The excitation laser beam is shaped into an 8 μm × 1 mm line that is focused along the direction of the PC grating, while remaining collimated perpendicular to the grating. Such a beam configuration offers high excitation power density while simultaneously providing high resonant coupling efficiency from the laser to the PC surface. Using a panel of 21 immunofluorescence assays on the PC surface in a microarray format, the approach achieves an enhancement factor as high as 90-fold between on-resonance and off-resonance illumination. The instrument provides a capability for sensitive and inexpensive analysis of cancer biomarkers in clinical applications.

OCIS codes: 050.5298, 180.2520, 130.5296.

Photonic crystal (PC) surfaces can provide predictably high enhancement of fluorescence as a result of amplified near-field and directional fluorescence emission [1–7]. For bioassays involving analytes at concentrations <1 pg/mL, the ability to enhance fluorescence intensity is desirable in order to reduce detection limits for a variety of surface-based fluorescent assays including DNA microarrays and protein micro-arrays [8–10].

PC-enhanced fluorescence (PCEF) exploits the resonant evanescent field that has an intensified local energy density compared to the excitation light source. A resonant mode of the PC is associated with a distinct resonant wavelength (λ_r) and resonant coupling angle (θ_r, ϕ_r). In our previous work, an illumination approach using an expanded and collimated laser beam efficiently coupled the light at λ_r into the target resonant mode [11,12] resulting in a fluorescence intensity enhancement of 600× compared to performing an identical assay on an unpatterned glass surface. While an expanded laser illumination source enables imaging of a large field of view, it provides relatively low power density compared to a focused laser beam, thus compromising detection sensitivity. This has prevented PCEF from significantly outperforming conventional confocal scanners and further lowering the detection limits for protein microarrays. In this Letter we present a viable solution to address this critical issue by utilizing a line-focused illumination scheme. We discuss a new design criterion for PCEF instrumentation by independently analyzing the PC photonic bands in two perpendicular planes. To demonstrate the instrument's fluorescence enhancement, we perform a protein microarray scan for simultaneous detection of 21 cancer biomarkers.

A schematic diagram of the PC structure used in this Letter is shown in Fig. 1(a). The one-dimensional (1D) grating structure was fabricated using nanoimprint lithography, which has been fully described in [4]. The PC structure has a period of $\Lambda = 400$ nm, duty cycle 50%, and a grating depth of $d = 50$ nm. The grating surface has a 130 nm thick TiO_2 dielectric thin film (refractive index, $n = 2.35$). Under broadband illumination, a highly efficient reflection represents a resonance at a specific wavelength and a specific angle. The photonic band diagrams of the PC were obtained by illuminating the device with collimated broadband light from a tungsten lamp. A spectrometer (USB 2000, Ocean Optics) was used to analyze the reflected light as a function of the incident angle in each illumination plane. The measured band diagrams are shown in Figs. 1(b) and 1(c) when the angle of incidence is scanned from 0° to 12° in ϕ (y-z plane) and θ (x-y plane) directions, respectively. Figure 1(b) shows the resonant wavelength change dramatically when the incident angle ($\theta = 0°$ and $0° < \phi < 12°$) varies perpendicular to the orientation of the grating. For a narrow bandwidth source, such as a solid-state laser (linewidth ~1 nm at $\lambda = 639$ nm),

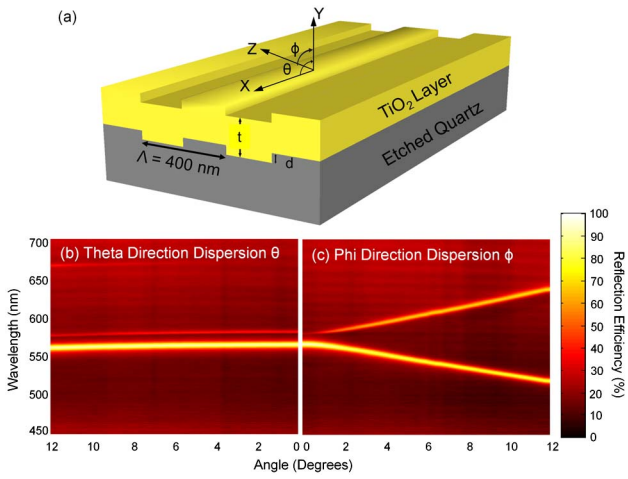

Fig. 1. (Color online) (a) Schematic of the PC structure (not to scale). The grating is oriented along the x-axis; (b) Photonic band diagram of the PC surface for $\phi = 0°$ and ϕ varied from 0° to 12°; (c) Photonic band diagram of the PC sensor for $\phi = 0°$ and ϕ varied from 0° to 12°.

a misalignment of the incidence angle by 0.1° with respect to the resonant angle ϕ_r will reduce the coupling efficiency to the PC by 10×. However, the photonic band diagram in Fig. 1(c) exhibits very small angular dependence (0.3 nm/ deg) along the θ direction. To efficiently couple light into the PC structure, the excitation laser source must match the resonance coupling condition dictated by the band diagram. The 1D structure of the PC chosen has a unique property that only demands the excitation laser beam be collimated and tuned along the ϕ direction, thus allowing focused illumination in the θ direction. The consequence of this beam profile is increased power density supplied to fluorescent dye molecules and a subsequent improvement in the fluorescence signal strength.

A schematic of the detection instrument is shown in Fig. 2(a). The excitation source is a single-mode fiber-coupled semiconductor laser diode (AlGaAs, 35 mW, $\lambda = 639$ nm). Since the PC structure is sensitive to the polarization of incident light, we used a polarizer to orient the polarization perpendicular to the direction of grating structure. The output from the fiber is collimated by an aspherical lens (L1, $f_{L1} = 30$ mm) and then focused by a cylindrical lens (C1, $f_{C1} = 6.35$ mm) at the focal point of L1 to a line 8 μm × 2 mm. The beam profile of the line is shown in Fig. 2(b). The profile along (z-direction) and across (x-direction) the line is plotted in Fig. 2(c), showing the expected Gaussian line shape in the direction of focus. The intensity variation across the line is <20%. The output end of the fiber is positioned at the focal plane of L1. Translation of the fiber in the direction perpendicular to the orientation of the grating enables adjustment of the incident angle (ϕ) from 0° to 20° with an accuracy of 0.02°. The incident angle in terms of the displacement (Δd) is given by $\phi = \tan^{-1}(\Delta d / f_{L1})$.

The line-shaped laser beam is orientated perpendicular to the PC grating. The power density of the beam is ~250× greater than the collimated-illumination instrument described previously [11]. The fluorescence emission is collected by a 2× objective lens (N.A. = 0.06) and quantified by an air-cooled linear CCD camera. The PC is placed on a motorized sample stage (MS2000, Applied Scientific Instruments) and translated perpendicular to the laser line for a fast scan (750 lines/second). The fluorescence image is constructed by sequential scanning across the sensor in 8 μm increments. A pixel resolution of 8 μm × 8 μm was used for all the fluorescence images reported in this Letter.

In Fig. 2(d) we characterize the fluorescence signal and the laser transmission efficiency through the PC as a function of ϕ. Coupling efficiency (lower transmission efficiency) with the PC directly influences fluorescence output.

As a demonstration, we performed a microspot immunofluorescence assay. The PC was prepared by immobilizing capture antibodies [shown in Fig. 1(a)] for 21 breast cancer biomarkers. The specific details of the microarray preparation and sandwich assay procedure (including the concentrations of specific antigens used) can be found in [8]. In brief, following the application of 3-glycidoxypropyl-trimethoxysilane using a vapor-phase deposition system, capture antibodies were diluted in phosphate buffered saline (PBS) to a

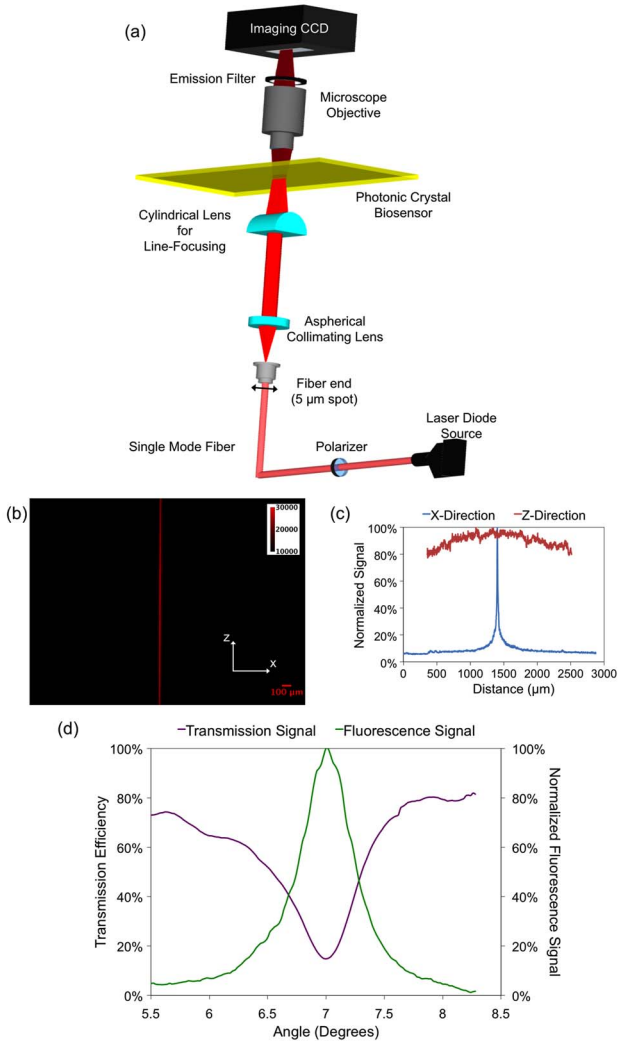

Fig. 2. (Color online) (a) Photonic crystal enhanced line-scanner schematic; (b) Image of the line on a two dimensional CCD showing a narrow tightly focused line; (c) The intensity profile along the line and across the line. The line has a Gaussian profile in both directions; (d) A curve showing a comparison of the coupling efficiency to the resonant mode for a line focused beam and the corresponding normalized fluorescence signal.

concentration of 0.8 mg/ml. Four replicate spots per assay were printed in each array on a 1 in. × 3 in. quartz PC slide using a noncontact printer. After a blocking step, the slide was incubated with a mixture of biomarkers (Table 1) and 0.1% casein in PBS with gentle agitation overnight. The slide was then incubated with a mixture of biotinylated detection antibodies at 25 ng/ml in PBS-tween (PBS-T) with mild agitation. Next the slide was incubated in a solution of 1 μg/ml SA-Cy5 in PBS-T. Finally, the slides were washed and dried.

The fluorescence enhancement capability of the line-scanning setup is demonstrated in the context of this microarray experiment. Fluorescence measurements were performed with the illumination angle configured for on-resonance or off-resonance excitation. The biomarker analytes and the respective concentrations are all listed in Table 1. The fluorescent images [shown in Figs. 3(a) and 3(b)] consist of 2082 pixels × 2016 lines

Table 1. Antigens and Concentrations

Antigen	Abbr.	Conc. ng/ml
Amphiregulin	AmR	3.33
Basic fibroblast growth factor	bFGF	3.33
CD14	CD14	16.67
Epidermal growth factor	EGF	0.83
Epidermal growth factor receptor	EGFR	4.17
E-selectin	Esel	4.17
Heparin-binding epidermal growth factor	HBEGF	0.83
c-erbB-2 extracellular domain	HER2	8.33
Hepatocyte growth factor	HGF	1.67
Intercellular adhesion molecule 1	ICAM	16.67
Insulin-like growth factor 1	IGF1	3.33
Matrix metalloprotease 1	MMP1	16.67
Matrix metalloprotease 2	MMP2	8.33
Matrix metalloprotease 9	MMP9	8.33
Platelet-derived growth factor AA	PDGF	1.25
Prostate specific antigen	PSA	1.67
Regulated on activation normal T cell expressed and secreted	RANTES	0.83
Transforming growth factor alpha	TGFα	0.83
Tumor necrosis factor alpha	TNFα	1.67
Urokinase-type plasminogen receptor	uPAR	8.33
Vascular endothelial growth factor	VEGF	3.33

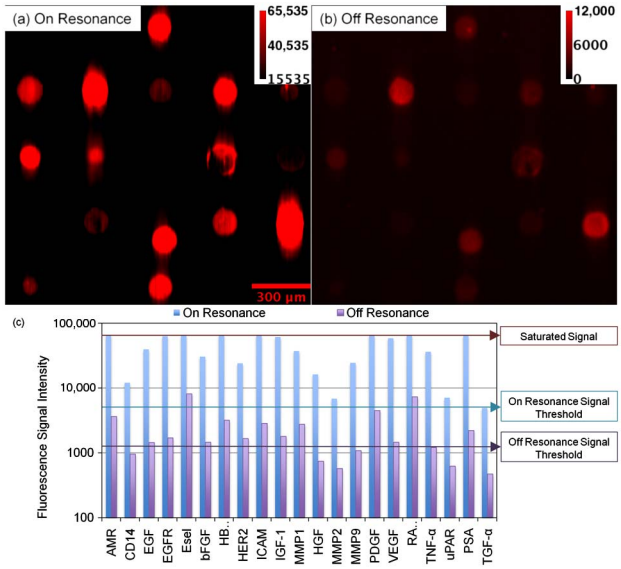

Fig. 3. (Color online) The images of the 21 assays are shown for both (a) on- and (b) off-resonance illumination; (c) The signal intensity on- and off-resonance for each assay measured using the developed line-scanner. The on-resonance and off-resonance signal thresholds are indicated.

with 16 bit grayscale resolution. The illumination angle was first tuned to $\phi = 20°$ and the microarray was scanned to obtain an off- resonance measurement. To perform the on-resonance measurement, the excitation angle (ϕ) was tuned to a value of $\phi = 7°$. Figure 3(c) also shows the fluorescence signal for both the on- and off-resonance cases on an assay-by-assay basis. Threshold values for detection above background noise for both the on- and off-resonance cases are indicated by the two horizontal lines on Fig. 3. In order to calculate the threshold values, it is necessary to characterize noise in terms of the standard deviation of the background signal. The background signal was defined as the localized intensity outside of the printed antibody spots. Each threshold value was calculated as three standard deviations above the average background signal. Selection of laser power, CCD gain, and integration time that allows measurement for both the on-resonance and off-resonance illumination is difficult. In Fig. 3(c), it is observed that while many assays in the off-resonance case are below the detection threshold, many on-resonance assays provide fluorescence intensity that is greater than the maximum intensity of the CCD. Considering only the assays that do not display a saturated response, the signal enhancement due to on-resonance illumination is ~90×.

We have reported on a new approach for optimized PC enhanced fluorescence. Our selection of a line-focused illumination approach is based on our analysis of the PC photonic bands. We highlighted the various critical design considerations that need to be addressed for optimal interfacing between a 1D PC and a line-focused illumination source. By using a microspot immunofluorescence assay on a PC, we demonstrated a raw signal enhancement of 90×. This enhancement factor is due only to the PC "enhanced excitation" effect, and does not include the additional effects of PC "enhanced extraction" of emitted photons, which has been shown to provide an additional ~10× enhancement factor [1,4,13]. This significant improvement in signal output is a consequence of the efficient coupling that is between a PC and the carefully designed line-scanning instrument.

This research was supported by the National Science Foundation (grant no. CBET 07-54122) and the National Institutes of Health (grant no. R01 GM086382). The first two authors contributed equally to this work.

References

1. N. Ganesh, W. Zhang, P. C. Mathias, E. Chow, J. Soares, V. Malyarchuk, A. D. Smith, and B. T. Cunningham, Nat. Nanotechnol. **2**, 515 (2007).
2. T. Kaji, T. Yamada, R. Ueda, and A. Otomo, J. Phys. Chem. Lett. **2**, 1651 (2011).
3. M. Li, P. Zhang, J. Li, J. Zhou, A. Sinitskii, V. Abramova, S. O. Klimonsky, and Y. D. Tretyakov, Appl. Phys. B **89**, 251 (2007).
4. A. Pokhriyal, M. Lu, V. Chaudhery, C.-S. Huang, S. Schulz, and B. T. Cunningham, Opt. Express **18**, 24793 (2010).
5. I. V. Soboleva, E. Descrovi, C. Summonte, A. A. Fedyanin, and F. Giorgis, Appl. Phys. Lett. **94**, 231122 (2009).
6. N. Ganesh, P. C. Mathias, W. Zhang, and B. T. Cunningham, J. Appl. Phys. **103**, 083104 (2008).
7. A. Brzezinski, J.-T. Lee, J. D. Slinker, G. G. Malliaras, P. V. Braun, and P. Wiltzius, Phys. Rev. B **77**, 233106 (2008).
8. C.-S. Huang, S. George, M. Lu, V. Chaudhery, R. Tan, R. C. Zangar, and B. T. Cunningham, Anal. Chem. **83**, 1425 (2011).
9. P. C. Mathias, S. I. Jones, H. Y. Wu, F. Yang, N. Ganesh, D. O. Gonzalez, G. Bollero, L. O. Vodkin, and B. T. Cunningham, Anal. Chem. **82**, 6854 (2010).
10. V. Chaudhery, C.-S. Huang, A. Pokhriyal, J. Polans, and B. T. Cunningham, Opt. Express **19**, 23327 (2011).
11. I. D. Block, P. C. Mathias, N. Ganesh, S. I. Jones, B. R. Dorvel, V. Chaudhery, L. O. Vodkin, R. Bashir, and B. T. Cunningham, Opt. Express **17**, 13222 (2009).
12. V. Chaudhery, M. Lu, A. Pokhriyal, S. Schulz, and B. Cunningham, IEEE Sens. J. **12**, 1272 (2011).
13. P. C. Mathias, H.-Y. Wu, and B. T. Cunningham, Appl. Phys. Lett. **95**, 021111 (2009).